European Neuropsychopharmacology (2020) 33, 58–70

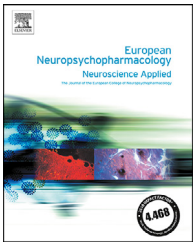

www.elsevier.com/locate/euroneuro

Structural and functional MRI of altered brain development in a novel adolescent rat model of quinpirole-induced compulsive checking behavior

Milou Straathof[a,*], Erwin L.A. Blezer[a], Caroline van Heijningen[a], Christel E. Smeele[a], Annette van der Toorn[a], TACTICS Consortium[1], Jan K. Buitelaar[b,c], Jeffrey C. Glennon[b], Willem M. Otte[a,d], Rick M. Dijkhuizen[a]

[a] *Biomedical MR Imaging and Spectroscopy Group, Center for Image Sciences, University Medical Center Utrecht and Utrecht University, Utrecht, the Netherlands*
[b] *Department of Cognitive Neuroscience, Donders Institute for Brain, Cognition and Behavior, Radboud University Medical Center, Nijmegen, the Netherlands*
[c] *Karakter Child and Adolescent Psychiatry University Center, Nijmegen, the Netherlands*
[d] *Department of Pediatric Neurology, UMC Utrecht Brain Center, University Medical Center Utrecht and Utrecht University, Utrecht, the Netherlands*

Received 19 August 2019; received in revised form 7 February 2020; accepted 17 February 2020

KEYWORDS
Adolescents;
Diffusion-weighted MRI;
Frontostriatal circuitry;
Obsessive compulsive disorder;
Quinpirole rat model;
Resting-state fMRI

Abstract
Obsessive-compulsive disorder (OCD) is increasingly considered to be a neurodevelopmental disorder. However, despite insights in neural substrates of OCD in adults, less is known about mechanisms underlying compulsivity during brain development in children and adolescents. Therefore, we developed an adolescent rat model of compulsive checking behavior and investigated developmental changes in structural and functional measures in the frontostriatal circuitry. Five-weeks old Sprague Dawley rats were subcutaneously injected with quinpirole ($n = 21$) or saline ($n = 20$) twice a week for five weeks. Each injection was followed by placement in the middle of an open field table, and compulsive behavior was quantified as repeated checking behavior. Anatomical, resting-state functional and diffusion MRI at 4.7T were conducted before the first and after the last quinpirole/saline injection to measure regional

* Corresponding author. Postal address: Heidelberglaan 100, 3584 CX Utrecht, the Netherlands.
E-mail address: M.Straathof-2@umcutrecht.nl (M. Straathof).
[1] Members of the TACTICS consortium are listed in the Acknowledgments.

https://doi.org/10.1016/j.euroneuro.2020.02.004

volumes, functional connectivity and structural integrity in the brain, respectively. After consecutive quinpirole injections, adolescent rats demonstrated clear checking behavior and repeated travelling between two open-field zones. MRI measurements revealed an increase of regional volumes within the frontostriatal circuits and an increase in fractional anisotropy (FA) in white matter areas during maturation in both experimental groups. Quinpirole-injected rats showed a larger developmental increase in FA values in the internal capsule and forceps minor compared to control rats. Our study points toward a link between development of compulsive behavior and altered white matter maturation in quinpirole-injected adolescent rats, in line with observations in pediatric patients with compulsive phenotypes. This novel animal model provides opportunities to investigate novel treatments and underlying mechanisms for patients with early-onset OCD specifically.

1. Introduction

Obsessive-compulsive disorder (OCD) is a mental illness in which people have recurrent thoughts, impulses or images that inflict anxiety, distress and repetitive behaviors. OCD has been recognized as a relatively common psychiatric disorder with a lifetime prevalence of 1–3% in the general population (Kessler et al., 2005; Veale and Roberts, 2014). Although the key symptoms are obsessions and compulsions, people suffering from OCD may experience substantial variation in the severity of symptoms, the time of onset and the effect of treatment (Butwicka and Gmitrowicz, 2010; Eisen et al., 2013; Leckman et al., 2010; Lochner and Stein, 2013). These variations in OCD manifestations suggest that there are multiple mechanisms that could underlie the development of this disorder. Nevertheless, in recent years a consistent picture has emerged that shows that OCD is associated with structural and functional changes in brain areas that form the frontostriatal circuitry. Neuroimaging modalities, including positron emission tomography, single-photon emission computed tomography and MRI, have been used to characterize these changes (Frydman et al., 2016; Koch et al., 2014; Piras et al., 2015). Although results are variable, studies in adults with OCD point to a decreased gray matter volume in frontal cortical regions such as the orbitofrontal, parietal and anterior cingulate cortex, and increased volume in subcortical structures such as the putamen, thalamus and caudate nucleus (Boedhoe et al., 2018; Piras et al., 2015; Radua and Mataix-Cols, 2009). Structural changes in main white matter tracts have also been reported in adults with OCD. Decreased fractional anisotropy (FA) values, potentially reflective of reduced white matter integrity, have been measured in several white matter tracts, of which the cingulate bundle, corpus callosum and internal capsule appear to be most commonly affected (Koch et al., 2014).

The OCD phenotype may not only be related to the above-mentioned changes in brain structures, but also to changes in neural network activation patterns. Functional imaging techniques have revealed abnormal activity in specific regions of the frontostriatal circuitry (Del Casale et al., 2011). Symptom provocation-induced hyper- and hypo-activity have been detected in the orbitofrontal cortex, the caudate nucleus, and the thalamus in adults and adolescents (Adler et al., 2000; Gilbert et al., 2009). Studies using resting-state functional MRI (rs-fMRI) have shown that functional connectivity between specific areas of the frontostriatal circuitry may be increased or decreased in people with OCD (Calzà et al., 2019; Posner et al., 2014; Sakai et al., 2011).

Despite increasing insights in neural substrates of OCD in adults, less is known about potential underlying mechanisms during brain development in children and adolescents. The first appearance of clinical symptoms divides the OCD population into two groups, i.e. early and late onset OCD patients that experience their first clinical symptoms before or after adulthood, respectively. The early onset group is the most prevalent since approximately three quarters of patients experience their first symptoms at a young age (Taylor, 2011). OCD may therefore be considered a neurodevelopmental disorder for the majority of affected persons.

In recent years a variety of translational animal models has been developed to study the pathophysiology of OCD and to test the effects of novel molecules (Albelda and Joel, 2012a, 2012b; Alonso et al., 2015). A frequently applied and well-defined model involves repeated injections of the dopamine D2/D3 receptor agonist quinpirole in adult rats (Szechtman et al., 1998). This results in sensitization of the D2/D3 receptor and compulsive checking behavior, a specific symptom of OCD. We set out to adapt this model to study the development of compulsive behavior during brain maturation in rats from juvenile to adolescent stages, with the specific goal to identify abnormal developmental changes in structural and functional aspects of the frontostriatal circuitry. To this aim, we applied serial structural and functional MRI of the brain, in combination with behavioral testing of compulsivity.

2. Experimental procedures

2.1. Animal model

All animal procedures were approved by the local Committee for Animal Experiments of the University Medical Center Utrecht, The Netherlands (DEC: 2014.I.12.104) and were performed in accordance with the guidelines of the European Communities council directive (EU Directive 2010/63/EU). All efforts were made to reduce animal suffering.

To study compulsive behavior in adolescent rats, we modified an established rat model for compulsive checking

behavior. Forty-one juvenile Sprague Dawley rats (Harlan, Zeist) were housed individually and habituated to environmental conditions (temperature 22–24° and 12 h light/dark cycle with lights on at 7:00 AM) for at least seven days prior to the experiment with access to food and water ad libitum. From the age of five weeks (body weight: 104 ± 24 g (mean $\pm$ standard deviation (SD))), we subcutaneously injected rats with quinpirole (Tocris, UK; 0.5 mg/kg; $n = 21$; Quinpirole group) or saline ($n = 20$; Control group), twice a week for five weeks (a total of 10 injections). We randomly assigned the treatment (quinpirole or saline), but experimenters could not be blinded, due to the obvious behavioral effects of quinpirole treatment. Each injection was followed by placement of the rat in the middle of a large open field table for 30 min. On the open field table (160×160 cm^2, 60 cm above the floor), four objects (two black, two white; $8 \times 8 \times 8$ cm^3) were placed on fixed locations: two near the middle and two near the corners of the open field. Each rat's activity on the open field table was recorded with a camera fixed to the ceiling.

2.2. Behavioral analysis

Ethovision software (Noldus Information Technology B.V., Netherlands) was used to automatically trace the trajectories of locomotion for the open field tests after the fifth and tenth quinpirole/saline injection. The open field area was virtually divided into 25 rectangles of 40×40 cm^2 of which the outer zones extended outside the open field. For all analyses, we used the last 15 min for the quinpirole-injected rats, and the complete 30 min for the control rats, similar to the original study by Szechtman and colleagues who used the last 30 of 60 min for quinpirole-injected rats and the full 60 min for control rats (Szechtman et al., 1998). We calculated the frequency of visits for each zone during this observation period and defined the home-base as the most frequently visited zone.

2.2.1. Locomotor behavior

Compulsive checking behavior parameters were characterized relative to the home-base, and included frequency of checking (the total number of visits at the home-base), length of checks (the average time of a visit at the home-base), recurrence time of checking (the average time spent at other areas before returning to the home-base) and stops before returning to the home-base (the average number of areas an animal visited before returning to the home-base) (Szechtman et al., 1998; Tucci et al., 2014). In addition, we determined the predictability of the visited zones as the Lempel-Ziv source entropy (Song et al., 2010) using a maximal substring of three zones and only including animals that visited at least nine different zones. The higher the source entropy, the less predictable the locomotion. Besides the compulsive behavior, we calculated hyperactivity measures, including the total travelled distance, average velocity of movement and immobility time (<0.01 cm movement per video frame).

2.2.2. Behavior during stops

We manually quantified stereotypic behaviors the rats showed during a stop at their own home-base (Szechtman et al., 1998). Like in the adult model, only the first 20 visits during the observation period were scored. However, because control rats were less active, all their visits were scored if required. First, for each visit we scored the entering or leaving direction to and from the home-base, to determine a potential directional preference. Directions were determined using a compass divided into eight different directions (per 45°). Second, we counted the number of clockwise and anti-clockwise turns as horizontal movements per visit and the number of head dips as vertical movements. Third, we scored the interaction of the rat with the object by counting the number of sniffs and placement of the forelegs at the object per visit. Fourth, we determined the grooming time per visit. These individual behavioral scores were combined into a total number of behavioral acts per visit.

2.3. Experimental MRI protocol

MRI experiments were done before the first and after the tenth injection of quinpirole or saline. MRI experiments were executed on a 4.7T horizontal bore magnet (Varian, Palo Alto, USA) with a homebuilt Helmholtz volume coil for radiofrequency transmission and an inductively coupled surface coil for signal detection.

Animals were anesthetized with isoflurane anesthesia (4% for induction and 2% for maintenance) in a mixture of O_2 and air (30/70%). Subsequently, the animals were prepared for mechanical ventilation by endotracheal intubation. Animals were immobilized in a specially designed stereotactic holder and cradle to minimize movement during the MRI experiment. During MRI, end-tidal CO_2 was continuously monitored, and body temperature was maintained at 37.0 ± 1.0 °C. An infrared sensor (Nonin Medical Inc., Plymouth, MN, USA) was attached to the hind paw to monitor the heart rate and blood oxygen saturation.

Anatomical MRI: For volumetric analyses and registration, we performed a 3D balanced steady-state free precession scan. Repetition time (TR) = 5 ms; echo time (TE) = 2.5 ms; flip angle 20°; three averages; four pulse angle shifts; field-of-view (FOV) = $40 \times 32 \times 24$ mm^3; acquisition matrix = $160 \times 128 \times 96$ points; resolution = 250 μm isotropic. Total acquisition time was ten minutes. Isoflurane anesthesia level was reduced to 1.5% at the start of the anatomical MRI acquisition, to lower the anesthetic depth for the following resting-state fMRI acquisition.

Resting-state functional MRI: For functional connectivity analyses, we acquired T2*-weighted blood oxygenation level-dependent images using a single shot multi-slice 2D gradient echo-echo planar imaging (EPI) sequence under 1.5% isoflurane anesthesia. TR = 700 ms; TE = 20 ms; FOV = 32×27.2 mm^2; acquisition matrix = 40×34 points; slice thickness = 0.80 mm, 17 slices, isotropic resolution of 800 μm, 850 images. The acquisition time was ten minutes. Resting-state fMRI acquisition was always started at 90 min after quinpirole injection, to standardize the effects of quinpirole across animals.

Diffusion MRI: For structural connectivity analyses we acquired multi-slice diffusion-weighted spin-echo images using four-shot EPI encoding. Diffusion MRI acquisition was performed under 2.0% of isoflurane anesthesia to minimize animal motion. Acquisition parameters were as follows: TR = 3000 ms; TE = 26.2 ms; FOV = 32×32 mm^2; acquisition matrix = 64×128 points; in plane resolution = 500×250 μm^2, slice thickness = 500 μm; 25 slices; $\delta/\Delta = 10.84/4$ ms; b-value = 1335 s/mm^2; 60 directions. The acquisition time was 65 min.

2.4. Data analyses MRI

2.4.1. Regions-of-interest

For the structural connectivity analyses, several white matter tracts, known to be affected in adults and children with OCD, were used as regions-of-interest (Fig. 1A): the external capsule (only the lateral part relative to the cingulum, 2.92 to 1.56 mm from bregma), the internal capsule (2.92 to −1.08 mm from bregma), the forceps minor of the corpus callosum (2.52 to 2.76 mm from bregma), the genu of the corpus callosum (1.80 to 2.28 mm from bregma) and the central part of the corpus callosum (defined as areas posterior to the genu of the corpus callosum (1.80 mm from bregma) and anterior to the dorsal part of the third ventricle (−0.60 mm from bregma, whereby only areas medial to the cingulum were included)).

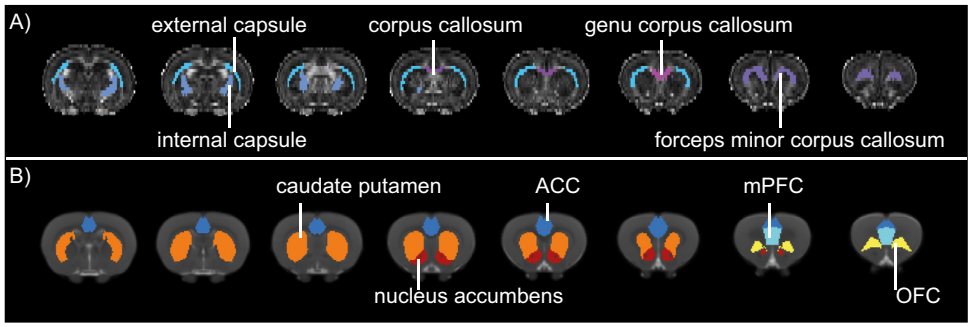

Fig. 1 Gray and white matter regions-of-interest. Regions-of-interest for the structural connectivity analyses projected on a fractional anisotropy (FA) map (A), and for the volumetric and functional connectivity analyses, projected on an anatomical image (B). For the functional connectivity analyses, frontal and striatal areas were combined into two regions-of-interest; the frontal cortex (consisting of the anterior cingulate, medial prefrontal and orbitofrontal cortex) and striatum (consisting of the nucleus accumbens and caudate putamen). ACC: anterior cingulate cortex; mPFC: medial prefrontal cortex; OFC: orbitofrontal cortex.

Regions of interest for the functional connectivity and volumetric analyses were taken from a 3D rendering of the Paxinos and Watson atlas (Paxinos and Watson, 2005). The 3D atlas rendering, with the region specifications and the corresponding MRI images, are available online (https://github.com/wmotte/rat_brain_atlas). We selected regions within the frontostriatal circuitry: the caudate putamen (CPu), nucleus accumbens (NAcc: accumbens nucleus shell, accumbens nucleus core and lateral accumbens shell), anterior cingulate cortex (ACC: cingulate cortex areas 1 and 2), medial prefrontal cortex (mPFC: prelimbic and infralimbic cortex) and orbitofrontal cortex (OFC: dorsolateral, lateral, medial and ventral orbital cortex) (Fig. 1B).

2.4.2. Diffusion MRI

The diffusion-weighted images were brain-extracted with BET and motion- and eddy current-corrected with mutual information-based affine transformations of all images to the baseline image (Mangin et al., 2002). The diffusion tensor, the corresponding eigensystem, and the subsequently derived fractional anisotropy (FA) was computed for each voxel within the brain mask (Basser and Pierpaoli, 1996). Mean FA values, reflecting the degree of anisotropy (degree of restricted diffusion along the main directions of the diffusion tensor), were calculated for all white matter tracts of interest at each time point as a measure of structural connectivity (Koay et al., 2006).

2.4.3. Resting-state functional MRI

Preprocessing steps of the resting-state fMRI scans included removal of the first 20 images to reach a steady state; motion-correction with MCFLIRT (Jenkinson et al., 2002); and brain-extraction with BET (Smith, 2002). Motion-correction parameters were used as regressor for the resting-state signal, and low-frequency blood oxygenation level-dependent fluctuations were obtained by applying temporal filtering between 0.01 and 0.1 Hz in AFNI (Cox, 1996). To verify the ability to measure specific functional connectivity under our experimental conditions, we evaluated the functional connectivity of the left anterior cingulate cortex from seed-based analyses. We calculated Fisher's Z-transformed correlation coefficients for inter- and intrahemispheric functional connectivity between regions-of-interest. To preserve sufficient signal-to-noise ratio for these analyses, we combined the orbitofrontal, anterior cingulate and medial prefrontal cortex into one frontal cortical region-of-interest, and the nucleus accumbens and caudate putamen into a striatal region. In addition, we performed functional connectivity analyses for the individual sub-regions of interest. The nucleus accumbens was excluded from this sub-region analysis, as the volume of this region in young rats was considered too small for reliable measurements.

2.4.4. Volumetric MRI

For the volumetric analyses of the regions of interest in the frontostriatal circuitry, we determined their volume in individual anatomical MRI space. For total gray matter and white matter volumes, we determined the volume in individual diffusion MRI space. The total cerebral white matter and gray matter volumes were calculated between the cerebellum and the olfactory bulb. For segmentation of the white matter we used a minimum FA threshold of 0.25, and for segmentation of the gray matter we used a maximum FA threshold of 0.25, and a mean diffusivity below 0.001. Total volumes were calculated by multiplying the number of voxels with the volume of a voxel in either anatomical or diffusion MRI space.

2.4.5. Matching individual data with atlas coordinates

Individual anatomical images were non-linearly registered with the atlas rendering using FNIRT software (Jenkinson et al., 2012). Individual resting-state fMRI and diffusion MRI images were linearly registered to the individual anatomical image using FLIRT software (Jenkinson and Smith, 2001), followed by the non-linear registration from the individual anatomical space to the atlas as described above. Regions-of-interest were transformed to individual anatomical, functional and diffusion MRI space by taking the inverse of these registrations. The regions for the functional connectivity analyses were masked with a temporal signal-to-noise ratio mask of 10, and the regions for the structural connectivity analyses were masked with a white matter mask (FA higher than 0.25 (Giannelli et al., 2010)).

2.5. Statistical analyses

Statistical analyses were performed in R (3.2.3) and R-studio 0.99 (R Core Team, 2014).

Differences in behavioral metrics (compulsive checking behavior, hyperactivity measures and behavior during stops) between control and quinpirole-injected rats after the fifth and tenth quinpirole/saline injection were analyzed with a Mann-Whitney U test.

We performed a mixed design ANOVA for all MRI parameters (regional brain volume, functional connectivity and structural connectivity) separately to assess brain development, with the factor *time* as within-subject variable, and treatment effect, with the

factor *group* (Control or Quinpirole) as between-subject variable, followed by post-hoc paired Wilcoxon signed rank tests. In addition, we determined whether MRI parameters significantly differed between control and quinpirole-injected rats after the tenth quinpirole/saline injection with Mann-Whitney U tests.

For all MRI-based measures we assessed possible correlation with compulsive behavior measures after the tenth quinpirole/saline injection in the quinpirole and control group separately, using linear regression.

All analyses were corrected for multiple testing using the false-discovery rate correction (Benjamini and Hochberg, 1995). Results with a corrected $p < 0.05$ were considered statistically significant.

3. Results

MRI acquisitions of two control and two quinpirole-injected rats were not complete, and behavioral data recording failed for two control rats and one quinpirole-injected rat. Therefore, final groups consisted of 18 quinpirole-injected and 16 control rats.

3.1. Locomotor, compulsive and grooming behavior

Fig. 2 shows a representative locomotor trajectory of one quinpirole-injected and one control rat after the tenth quinpirole/saline injection and the compulsive checking behavioral metrics that were calculated from the motor trajectories after the fifth and tenth quinpirole/saline injection. Compared to control rats, quinpirole-injected rats travelled more repeatedly between two zones of the open field (Fig. 2A and B). Both after the fifth and after the tenth quinpirole/saline injection, quinpirole-injected rats showed a higher frequency of checks (fifth injection: Control: 12.7 ± 6.6 (mean $\pm$ standard deviation (SD)); Quinpirole: 24.1 ± 12.3; $p = 0.003$; tenth injection: Control: 15.9 ± 9.4; Quinpirole: 51.6 ± 33.6; $p = 0.0004$), lower recurrence time of checking (fifth injection: Control: 122.4 ± 83.7 s; Quinpirole: 33.6 ± 29.0 s; $p = 0.0003$; tenth injection: Control: 115.5 ± 69.2 s; Quinpirole: 18.9 ± 10.8 s; $p < 0.0001$) and lower number of stops before returning to the home-base (fifth injection: Control: 10.1 ± 3.4; Quinpirole: 5.8 ± 2.0; $p < 0.0001$; tenth injection: Control: 10.6 ± 3.4; Quinpirole: 6.9 ± 1.7; $p = 0.0004$) than control rats (Fig. 2C). The average length of a visit at the home-base was not statistically significantly different between quinpirole-injected and control rats after the fifth (Control: 71.8 ± 91.1 s; Quinpirole: 25.7 ± 65.5 s; $p = 0.10$) and tenth quinpirole/saline injection (Control: 42.6 ± 84.4; Quinpirole: 6.3 ± 10.4; $p = 0.08$) (Fig. 2C).

The entropy of the visited zones was lower in quinpirole-injected rats compared to control rats after both the fifth and tenth injection (fifth injection: Control: 2.2 ± 0.005; Quinpirole: 2.0 ± 0.2; $p = 0.002$; tenth injection: Control: 2.2 ± 0.006; Quinpirole: 2.1 ± 0.007; $p < 0.0001$). This lower entropy in quinpirole-injected rats means that the order of visited zones is less random and shows a higher degree of predictability and repeatability.

Next to compulsive behavior, we characterized hyperactivity measures in control and quinpirole-injected rats after the fifth and tenth quinpirole/saline injection (Fig. 2D). At both time-points, quinpirole-injected rats moved with a higher mean velocity (fifth injection: Control: 2.8 ± 1.3 cm/s; Quinpirole: 6.6 ± 3.6 cm/s; $p = 0.0004$; tenth injection: Control: 3.3 ± 1.5 cm/s; Quinpirole: 11.7 ± 5.1 cm/s; $p = 0.002$) and had a lower immobility time (fifth injection: Control: 495.4 ± 207.8 s; Quinpirole: 47.2 ± 41.4 s; $p < 0.0001$; tenth injection: Control: 519.1 ± 236.7 s; Quinpirole: 22.1 ± 18.0 s; $p < 0.0001$). After the tenth quinpirole/saline injection, the quinpirole-injected rats moved over a longer distance (Control: 5954 ± 2664 cm; Quinpirole: $11{,}112 \pm 5454$ cm; $p = 0.002$). The total distance moved was not significantly different between quinpirole-injected and control rats after the fifth quinpirole injection (Control: 4963 ± 2316 cm; Quinpirole: 5899 ± 3178 cm; $p = 0.34$).

After the fifth injection, control rats groomed significantly more during a visit of the home-base than quinpirole-injected rats (Fig. 2E; Control: 6.7 ± 8.7 s; Quinpirole: no detectable grooming; $p = 0.004$). The average grooming time per visit was not significantly different between control and quinpirole-injected rats after the tenth injection, although quinpirole-injected rats did not groom at all (Control: 1.21 ± 2.40 s; $p = 0.21$). All other behaviors we quantified during home-base visits were not statistically significantly different between quinpirole-injected and control rats at both time-points.

3.2. Structural integrity and functional connectivity

Fig. 3A and B show the structural connectivity in the white matter tracts of interest and the functional connectivity within the frontostriatal system, respectively, before the first and after the tenth quinpirole/saline injection.

For the structural integrity analyses, the mixed design ANOVA demonstrated a significant main effect of time for all included white matter tracts ($p < 0.0001$). Correspondingly, the post-hoc analyses revealed an increased FA value in all white matter tracts of interest in the control and quinpirole group after the tenth quinpirole/saline injection ($p < 0.0001$; Fig. 3A). In addition, the mixed design ANOVA showed a significant interaction effect of group and time for the internal capsule and the forceps minor, indicating that the change in FA over time in these white matter tracts was different between quinpirole-injected and control rats. The increase in FA over time in these two white matter areas was larger in quinpirole-injected rats than in control rats (internal capsule: Control: 0.041 ± 0.019; Quinpirole: 0.063 ± 0.019; $p = 0.007$; forceps minor: Control: 0.035 ± 0.016; Quinpirole: 0.053 ± 0.019; $p = 0.01$). After the tenth quinpirole/saline injection, we found trends towards higher FA values in quinpirole-injected vs. control rats in the internal capsule (Control: 0.45 ± 0.01; Quinpirole: 0.46 ± 0.01; $p = 0.06$), the forceps minor (Control: 0.44 ± 0.008; Quinpirole: 0.45 ± 0.01; $p = 0.14$) and the center of the corpus callosum (Control: 0.52 ± 0.03; Quinpirole: 0.53 ± 0.02; $p = 0.14$).

Seed-based analysis of functional connectivity of the left anterior cingulate cortex showed that our approach enabled

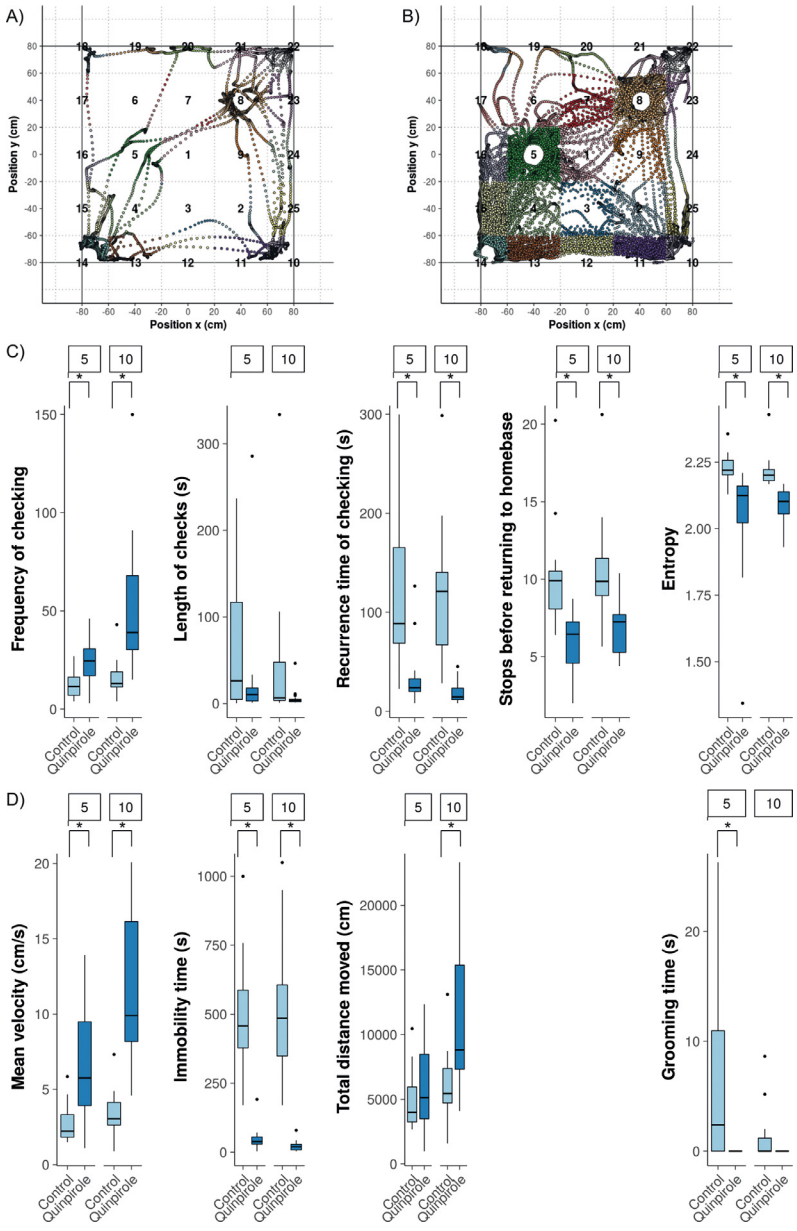

Fig. 2 Locomotor trajectories and compulsive and hyperactive behavioral metrics for control and quinpirole-injected adolescent rats during the open field test. Locomotor trajectory of a control (A) and a quinpirole-injected adolescent rat (B). The different zones of the open field are numbered, and the locomotor trajectories are colored corresponding to these zones. We characterized behavior during the open field test for the last 15 min for quinpirole-injected rats and the full 30 min for control rats. Boxplots of compulsive behavior, including the frequency of checking (total number of visits at the home-base during observation), length of checks (average time (s) spent at the home-base), recurrence time of checking (average time (s) before returning to the home-base), stops before returning to the home-base (average number of zones visited in between two visits at the home-base) and entropy (predictability of the visited zones) for control and quinpirole-injected rats after the fifth and tenth injection of quinpirole/saline (C). Boxplots of hyperactive behavior, including the mean velocity, immobility time (<0.01 cm movement per video frame) and the total distance moved for control and quinpirole-injected rats after the fifth and tenth injection of quinpirole/saline (D). Grooming time (average time (s) grooming per visit at the home-base) for control and quinpirole-injected rats after the fifth and tenth injection of quinpirole/saline (E). * corrected $p < 0.01$. Error bars represent the interquartile range and dots represent outliers. (For interpretation of the references to colour in this figure legend, the reader is referred to the web version of this article.)

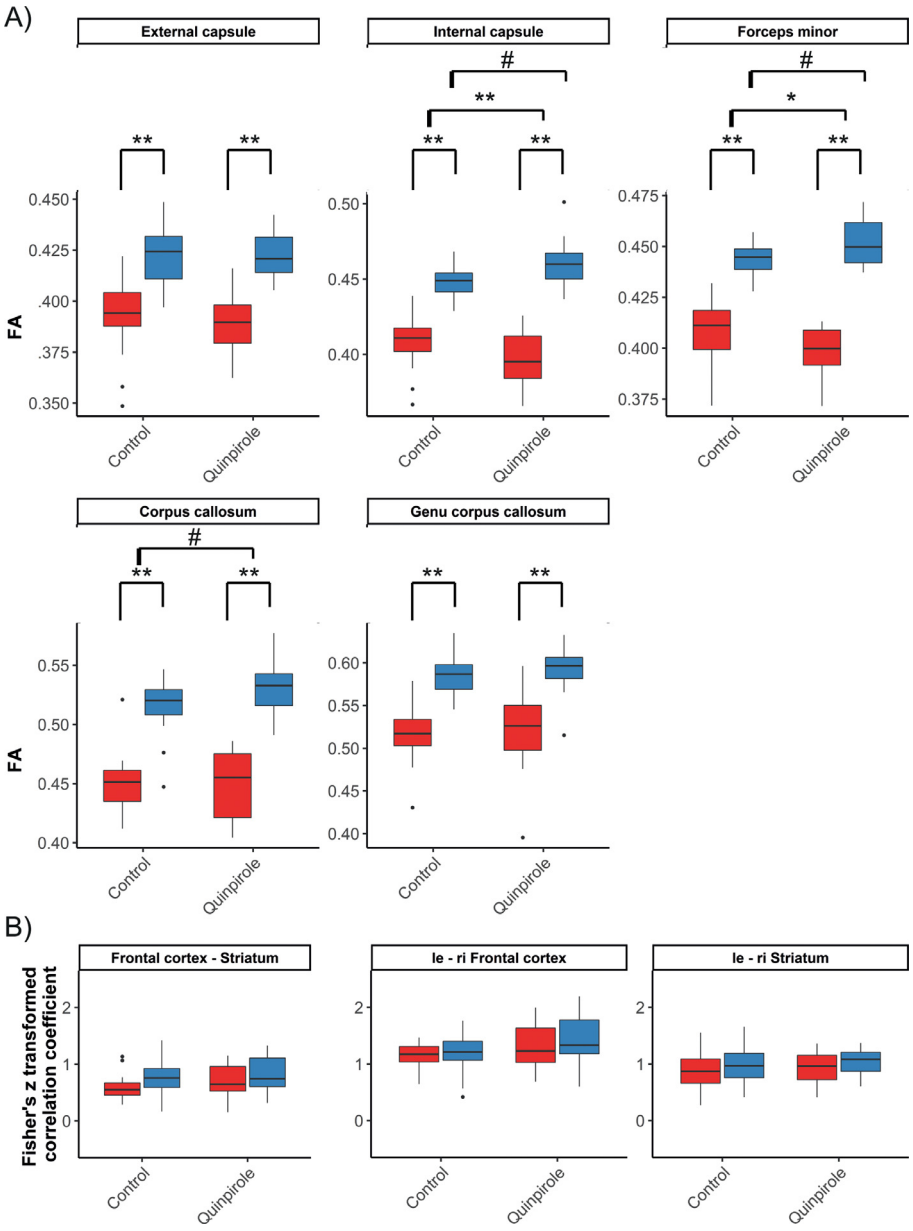

Fig. 3 Structural integrity and functional connectivity in control and quinpirole-injected rats before and after repeated saline/quinpirole injections. Structural integrity (A; fractional anisotropy (FA)) in white matter tracts of interest and functional connectivity (B; Fisher's Z transformed correlation coefficient) within the frontostriatal system for control and quinpirole-injected rats before the first (5-weeks old rats; red) and after the tenth (10-weeks old rats; blue) quinpirole/saline injection. le: left; ri: right. Error bars represent 1.5 × the interquartile range and dots represent outliers. ** corrected $p < 0.01$; * corrected $p < 0.05$; # corrected $p < 0.15$. (For interpretation of the references to colour in this figure legend, the reader is referred to the web version of this article.)

measurement of specific and localized functional connectivity effects in quinpirole-injected and control rats (Supplementary Fig. S1). The mixed design ANOVA, with the factor time as within-subject variable, and the factor group as between-subject variable, demonstrated a significant main effect of group, irrespective of time, for the interhemispheric connection between the two frontal cortices ($p = 0.01$). However, post-hoc analyses did not reveal statistically significant differences in interhemispheric frontal connectivity between quinpirole-injected and control rats after the tenth quinpirole/saline injection. In addition, we did not find any time or interaction effects, or differences between quinpirole-injected and control rats after the tenth quinpirole/saline injection. Functional connectivity analyses in individual sub-regions, also did not reveal significant differences between quinpirole-injected and control rats after the tenth quinpirole/saline injection (Supplementary Fig. S2).

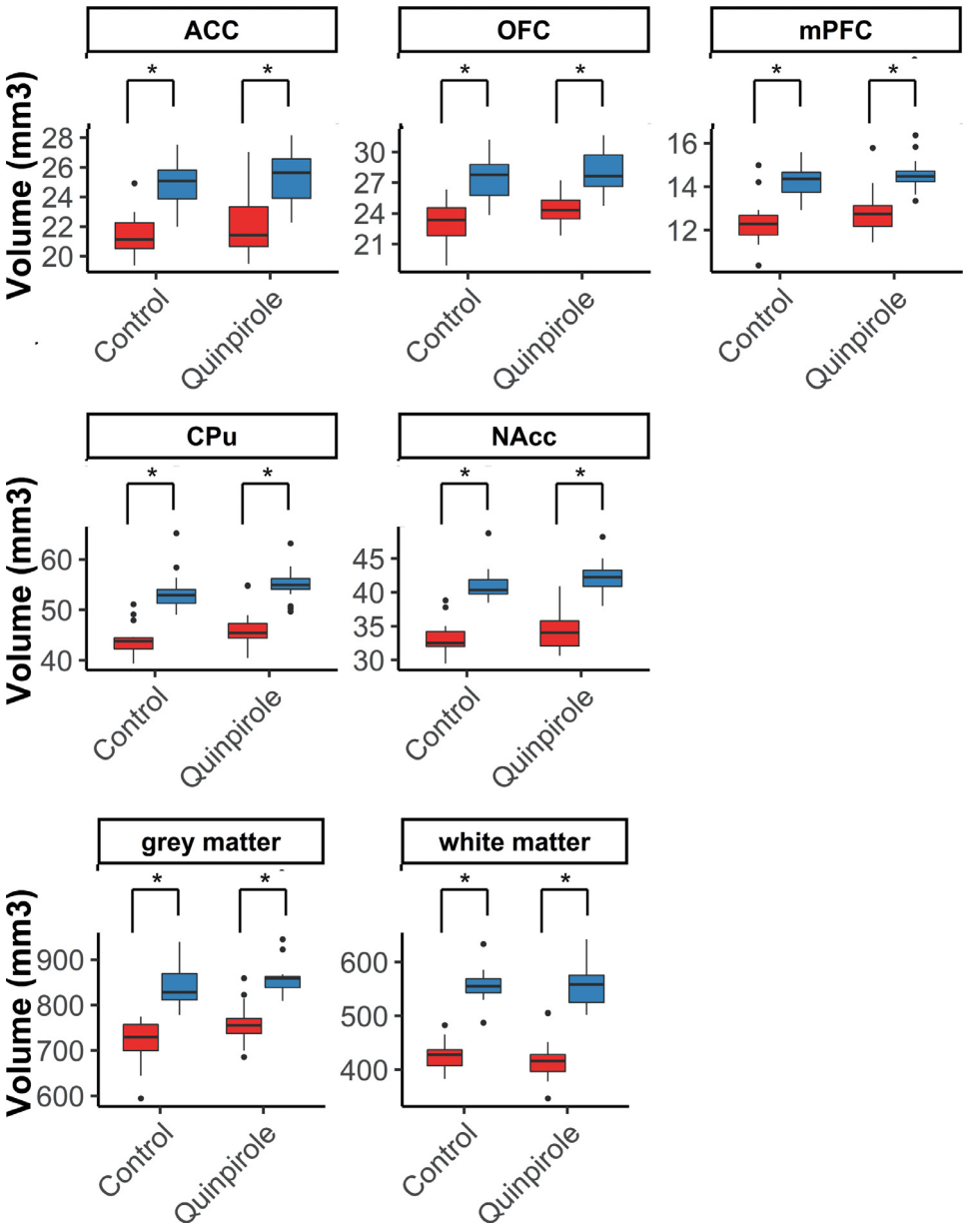

Fig. 4 Regional brain volumes before and after repeated quinpirole/saline injections. Boxplots of the volumes (mm^3) of regions-of-interest in the frontostriatal system, and the total white and gray matter volume for control and quinpirole-injected rats before the first (5-weeks old rats; red) and after the tenth injection (10-weeks old rats; blue) of quinpirole/saline. Error bars represent 1.5 × interquartile range and dots represent outliers. ACC: anterior cingulate cortex; OFC: orbitofrontal cortex; mPFC: medial prefrontal cortex; CPu: caudate putamen; NAcc: nucleus accumbens. * corrected $p < 0.01$. (For interpretation of the references to colour in this figure legend, the reader is referred to the web version of this article.)

3.3. Regional brain volumes

The volumes of regions within the frontostriatal system and the total gray and white matter volumes were determined before the first and after the tenth quinpirole/saline injection (Fig. 4). The mixed design ANOVA, with the within-subject factor time and between-subject factor group, demonstrated a significant time effect for all volumes of interest ($p < 0.0001$). Correspondingly, post-hoc analyses revealed that all the investigated cerebral volumes increased between the first (before the first injection) and the final measurement (after the tenth injection), in the saline- and quinpirole-injected groups ($p < 0.0001$; Fig. 4). There was no significant interaction effect between time and group. In addition, after the tenth quinpirole/saline injection, there were no significant differences in regional volumes between quinpirole-injected and control rats.

3.4. Relationship between compulsive behavior and MRI measures

We checked for possible relationships between MRI-based parameters and compulsive behavior measures after the tenth quinpirole/saline injection in the control and quinpirole group. None of the regressions demonstrated a significant correlation.

4. Discussion

We conducted a multi-parametric MRI examination of the development of compulsive behavior in a novel adolescent rat model of quinpirole-induced compulsive checking behavior. After five weeks of consecutive quinpirole injections, adolescent rats demonstrated clear compulsive checking behavior, repeated travelling between two open-field zones and no grooming. Our MRI measurements revealed developmental increases in regional brain volumes and white matter integrity in control and quinpirole-injected rats. Quinpirole-injected rats showed a larger increase in FA values in the internal capsule and forceps minor as compared to control rats, and a trend towards higher integrity values in the internal capsule, forceps minor and central part of the corpus callosum after five weeks of quinpirole treatment as compared to saline treatment.

4.1. Compulsive-like behavioral phenotype

While the model of quinpirole-induced compulsive checking in adult rats has shown good face validity to OCD (Stuchlik et al., 2016), compulsive behavior and OCD in humans generally develops during early adolescence (Boileau, 2011). Therefore, we have adapted the quinpirole-induced compulsive checking model in adult rats by starting quinpirole injections during early adolescence. Our study shows that quinpirole-injected adolescent rats meet three of four reported criteria for compulsive checking behavior after the fifth and tenth quinpirole/saline injection (Szechtman et al., 1998; Tucci et al., 2014). By including the measurement after the fifth quinpirole/saline injection (8–9 weeks of age), we assured that the compulsive behavior developed during the adolescent phase and was established before adulthood. An additional feature that we observed in the quinpirole-injected adolescent rats was repeated traveling between two sides of the open field. This is also observable in adult rats with an OCD-like phenotype (Eilam, 2017). Next to these compulsive checking behaviors, we also characterized hyperactivity measures and specific behavioral acts the rats performed during a visit at the home-base. Quinpirole-injected adolescent rats travelled over a longer total distance and with higher velocity than control rats, corresponding to hyperactivity, which has also been observed in the adult model (Servaes et al., 2019). In addition, in contrast to control animals showing clear grooming behavior during a home-base visit, quinpirole-injected adolescent rats did not groom, similar to what has been observed in the adult rat model (Szechtman et al., 1998). However, other behavioral acts, such as interaction with objects or preferences for entering or leaving directions, that were significantly altered in the adult model, were not significantly different between quinpirole-injected and control adolescent rats.

The development of compulsive-like behavior after repeated quinpirole injections is believed to reflect modifications in the brain due to the sensitization to the dopamine D2-receptor agonist quinpirole (Tucci et al., 2014), such as an increased D2 receptor density (Servaes et al., 2019). The reduced expression of compulsive checking behavior in the adolescent rat model may be explained by maturational differences in dopaminergic receptors in the striatum between day 40 (adolescence) and day 60 (adulthood) (Teicher et al., 1995), potentially resulting in reduced sensitivity to dopaminergic agonists in young rats (Bolanos et al., 1998; Ulloa et al., 2004). Nevertheless, we feel that the behavioral profile that we observed in response to repeated quinpirole injections during adolescence in rats effectively reflects a compulsive-like phenotype.

4.2. Structural and functional brain alterations

MRI-based measures of regional brain volume and white matter structural integrity revealed clear developmental changes in quinpirole-injected and control rats between pre- (early adolescence) and post-treatment (late adolescence/adulthood) time-points. The volumes of regions within the frontostriatal system, as well as the total gray and white matter volume, significantly increased during this developmental phase of adolescence. These findings are in line with previous research demonstrating that cortical and subcortical regions increase in volume up to at least two months of age in rats (Calabrese et al., 2013; Mengler et al., 2014), representing maturation of brain regions. White matter structural integrity also changed during this developmental period. We found increasing FA values in white matter tracts, between postnatal weeks five and ten. Previous studies also demonstrated an increase in FA values of white matter tracts during development in rats (Bockhorst et al., 2008; Calabrese and Johnson, 2013), which may continue during (early) adulthood (van Meer et al., 2012). Likewise, in humans, developmental increases in FA values of white matter tracts have been demonstrated to continue until the end of adolescence or the beginning of adulthood (Barnea-Goraly et al., 2005; Chen et al., 2016). These increasing FA values in white matter tracts during development may reflect ongoing myelination (Bockhorst et al., 2008). The increased FA values at postnatal week 10 may have resulted in more voxel inclusions and hence an apparent increase in white matter volume over time. Nevertheless, white matter volumes calculated from different MRI scans (not solely based on FA values) have been demonstrated to increase up until postnatal week 19 (Otte et al., 2015). Therefore, we believe that the white matter volume increase during development, as observed in the current study, is not merely explained by increased FA values over time, but truly reflects an increase in white matter volume.

Regional brain volumes and functional connectivity within the frontostriatal system did not differ between quinpirole-injected and control rats after the tenth quinpirole/saline

injection. In children with OCD, conflicting results have been reported regarding brain volume and functional connectivity changes. Increases or decreases, or even no differences, in the size of frontal cortical areas have been measured (Boedhoe et al., 2018; Christian et al., 2008; Lázaro et al., 2009). Furthermore, increased as well as decreased functional connectivity between frontostriatal regions has been reported (Bernstein et al., 2016; Fitzgerald et al., 2011). These differences may be related to the heterogeneous nature of OCD but could also be due to methodological variation between studies. This underscores the need for standardization of neuroimaging protocols and investigations in well-controlled experimental designs.

The developmental rise in FA in the internal capsule and forceps minor was larger in quinpirole-injected animals as compared to controls, suggesting differences in white matter maturation. As a result, we found a trend towards higher FA values in these white matter tracts and in the center of the corpus callosum in quinpirole-injected as compared to saline-injected rats after the five weeks treatment period. Elevated FA values in white matter tracts, including the corpus callosum and internal capsule, have also been observed in children and adolescents with OCD (Gruner et al., 2012; Zarei et al., 2011). The higher FA values in children with OCD are suggested to reflect premature myelination of white matter tracts (Zarei et al., 2011). In addition, FA values in the internal capsule have been shown to be positively correlated to symptom severity in children with OCD (Zarei et al., 2011). Together, these findings underline the involvement of white matter structural integrity disturbances in disease processes of OCD in children and adolescents.

The rat model of quinpirole-induced OCD-like behavior offers opportunities for standardized and well-controlled investigation of the neural underpinnings of compulsive checking behavior. Since approximately three quarters of patients experience their first symptoms at a young age (Taylor, 2011), the adolescent quinpirole rat model described in this study enables studying the neurodevelopmental processes underlying early-onset OCD specifically. For optimal translation, we used similar MR protocols as in human neuroimaging studies, including diffusion MRI and resting-state functional MRI. However, diffusion-based measures are proxies of the true neuroanatomical features, and the (sub)cellular processes underlying changes in FA remain largely unclear (Johansen-Berg and Behrens, 2013). In addition, in contrast to human neuroimaging studies, animals in our study were anesthetized during MRI acquisitions, which is known to influence functional connectivity measurements (Paasonen et al., 2018).

Despite the good face validity of the adult quinpirole-induced compulsivity model, its construct and predictive validity have not yet been extensively validated. The adolescent quinpirole-induced compulsive checking behavior model introduced in this study demonstrated face validity with regards to compulsive checking behavior and construct validity from disturbances in white matter integrity. However, despite clear behavioral effects, we did not find quinpirole-induced effects on resting-state functional connectivity. Quinpirole effects should still be present during the time of resting-state fMRI (90 min after injection) as the half-life time of quinpirole in rat plasma is 9.5 h (Whitaker and Lindstrom, 1987) and behavioral effects of quinpirole have been measured up to two hours after injection (Eilam et al., 1989). It may be that the use of anesthesia during our MRI acquisition has covered the effects of quinpirole on MRI-based measures of functional connectivity. Isoflurane anesthesia has been shown to affect the binding of agonistic PET tracers to the dopamine D2/D3 receptor (McCormick et al., 2011). Since quinpirole is a D2/D3 receptor agonist, the use of isoflurane anesthesia may have influenced the effects of quinpirole. Nonetheless, we expect a minimal contribution of this mechanism on the functional connectivity measurements in our study, since we administered quinpirole nine times without isoflurane anesthesia, and once at 40 min before the induction of isoflurane anesthesia. The clear behavioral effects in quinpirole-injected rats may be a direct result of the preceding quinpirole injection, rather than from a change in the macro-scale functional or structural brain connections. Since previous studies have shown abnormalities at the neurotransmitter and receptor level in the quinpirole model (Servaes et al., 2019, 2017), differences in structural and functional connectivity may be more subtle and at the micro-scale. Differences that are not detectable with macro-scale MRI-based measures. In addition, we cannot completely rule out that motion- and physiological-related noise may have obscured model-related changes in structural and functional connectivity. Future studies could investigate the predictive validity of the adolescent quinpirole model by assessing the effects of pharmacological treatments that are already used for children and adolescents with OCD. In addition, the adolescent quinpirole-induced compulsivity model provides unique opportunities to study potential novel therapeutic strategies and their working mechanisms for this subgroup of OCD patients specifically.

In conclusion, we found clear development of compulsive-like behavior and altered white matter maturation in a novel model of quinpirole-induced compulsivity in adolescent rats, which matched with reported substrates of early-onset OCD. Our study shows that MRI in animal models of specific symptoms of heterogeneous psychiatric disorders provides unique opportunities to assess the neurodevelopmental aspects and neurobiological substrates of these symptoms in a well-controlled experimental design.

Role of Funding Source

This work was supported by the Netherlands Organization for Scientific Research (dr. R.M. Dijkhuizen: NWO-VICI 016.130.662, dr. W.M. Otte: NWO-VENI 016.168.038), and the Dutch Brain Foundation (dr. W.M. Otte: F2014(1)-06). The research leading to these results has received funding from the European Community's Seventh Framework Program (FP7/2007–2013) TACTICS under grant agreement no. 278948. All funding sources have had no further role in study design; in the collection, analyses and interpretation of data; in the writing of the report; and in the decision to submit the paper for publication.

Contributors

Erwin L.A. Blezer, Jeffrey C. Glennon, Annette van der Toorn and Rick M. Dijkhuizen designed the study and wrote the protocol. Erwin L.A. Blezer and Caroline van Heijningen performed the experiments. Milou Straathof, Christel E. Smeele and Willem M. Otte analyzed the data. Milou Straathof wrote the first draft of the manuscript. Jan K. Buitelaar, Rick M. Dijkhuizen and Jeffrey C. Glennon provided extensive feedback to the manuscript. All authors contributed to and have approved the final manuscript.

Conflict of interest

All of the authors declare that they have no conflicts of interest.

Acknowledgments

This paper reflects only the author's views and the European Union is not liable for any use that may be made of the information contained therein.

The TACTICS consortium consists of Jan Buitelaar, Saskia de Ruiter, Jilly Naaijen, Sophie Akkermans, Maarten Mennes, Marcel Zwiers, Shahrzad Ilbegi, Leonie Hennissen, Jeffrey Glennon, Ilse van de Vondervoort, Katarzyna Kapusta, Natalia Bielczyk, Houshang Amiri, Martha Havenith, Barbara Franke, Geert Poelmans, Janita Bralten, Tom Heskes, Elena Sokolova, Perry Groot from Radboud University Medical Center Nijmegen, the Netherlands; Steven Williams, Declan Murphy, David Lythgoe, Muriel Bruchhage, Iulia Dud, Bogdan Voinescu from King's College London, United Kingdom; Ralf Dittmann, Tobias Banaschewski, Daniel Brandeis, Konstantin Mechler, Ruth Berg, Isabella Wolf, Alexander Häge, Michael Landauer, Sarah Hohmann, Regina Boecker-Schlier, Matthias Ruff from Central Institute of Mental Health, University of Heidelberg, Mannheim, Germany; Rick Dijkhuizen, Erwin Blezer, Milou Straathof, Kajo van der Marel, Pim Pullens, Wouter Mol, Annette van der Toorn, Willem Otte, Caroline van Heijningen, Sarah Durston, Vincent Mensen, Bob Oranje, René Mandl from University Medical Center Utrecht, Utrecht, the Netherlands; Daphna Joel from Tel Aviv University, Tel Aviv, Israel; John Cryan from University College Cork, Cork City, Ireland; Tracey Petryshen, David Pauls, Mai Saito from Massachusetts General Hospital, Boston, MA, USA; Angelique Heckman from Genoway, Lyon, France; Sabine Bahn from University of Cambridge, Cambridge, United Kingdom; Ameli Schwalber from concentris research management GmbH, Fürstenfeldbruck, Germany; and Ioana Florea from Lundbeck, Valby, Denmark.

Supplementary materials

Supplementary material associated with this article can be found, in the online version, at doi:10.1016/j.euroneuro.2020.02.004.

References

Adler, C.M., McDonough-Ryan, P., Sax, K.W., Holland, S.K., Arndt, S., Strakowski, S.M., 2000. fMRI of neuronal activation with symptom provocation in unmedicated patients with obsessive compulsive disorder. J. Psychiatr. Res. 34, 317–324. doi:10.1016/S0022-3956(00)00022-4.

Albelda, N., Joel, D., 2012a. Current animal models of obsessive compulsive disorder: an update. Neuroscience 211, 83–106. doi:10.1016/j.neuroscience.2011.08.070.

Albelda, N., Joel, D., 2012b. Animal models of obsessive-compulsive disorder: exploring pharmacology and neural substrates. Neurosci. Biobehav. Rev. 36, 47–63. doi:10.1016/j.neubiorev.2011.04.006.

Alonso, P., López-Solà, C., Real, E., Segalàs, C., Menchón, J.M., 2015. Animal models of obsessive-compulsive disorder: utility and limitations. Neuropsychiatr. Dis. Treat. 11, 1939–1955. doi:10.2147/NDT.S62785.

Barnea-Goraly, N., Menon, V., Eckert, M., Tamm, L., Bammer, R., Karchemskiy, A., Dant, C.C., Reiss, A.L., 2005. White matter development during childhood and adolescence: a cross- sectional diffusion tensor imaging study. Cereb. Cortex 15, 1848–1854. doi:10.1093/cercor/bhi062.

Basser, P., Pierpaoli, C., 1996. Microstructural and physiological features of tissue elucidated by quantitative-diffusion tensor MRI. J. Magn. Reson. Series B I 209–219.

Benjamini, Y., Hochberg, Y., 1995. Controlling the false discovery fate: a practical and powerful approach to multiple testing. J. R. Stat. Soc. Ser. B 57, 289–300.

Bernstein, G.A., Mueller, B.A., Westlund Schreiner, M., Campbell, S.M., Regan, E.K., Nelson, P.M., Houri, A.K., Lee, S.S., Zagoloff, A.D., Lim, K.O., Yacoub, E.S., Cullen, K.R., 2016. Abnormal striatal resting-state functional connectivity in adolescents with obsessive-compulsive disorder. Psychiatry Res. Neuroimaging 247, 49–56. doi:10.1016/j.pscychresns.2015.11.002.

Bockhorst, K.H., Narayana, P.A., Liu, R., Ahobila-Vijjula, P., Ramu, J., Kamel, M., Wosik, J., Bockhorst, T., Hahn, K., Hasan, K.M., Perez-Polo, J.R., 2008. Early postnatal development of rat brain: in vivo diffusion tensor imaging. J. Neurosci. Res. 86, 1520–1528. doi:10.1002/jnr.21607.

Boedhoe, P.S.W., Schmaal, L., Abe, Y., Alonso, P., Ameis, S.H., Anticevic, A., Arnold, P.D., Batistuzzo, M.C., Benedetti, F., Beucke, J.C., Bollettini, I., Bose, A., Brem, S., Calvo, A., Calvo, R., Cheng, Y., Cho, K.I.K., Ciullo, V., Dallaspezia, S., Denys, D., Feusner, J.D., Fitzgerald, K.D., Fouche, J.-.P., Fridgeirsson, E.A., Gruner, G., Hanna, G.L., Hibar, D.P., Hoexter, M.Q., Hu, H., Huyser, C., Jahanshad, N., James, A., Kathmann, N., Kaufmann, C., Koch, K., Soo Kwon, J., Lazaro, L., Lochner, C., Marsh, R., Martinez-Zalacain, I., Mataix-Cols, D., Menchon, J.M., Minuzzi, L., Morer, A., Nakamae, T., Nakao, T., Narayanaswamy, J.C., Nishida, S., Nurmi, E., O'Neill, J., Piacentini, J., Piras, F., Piras, F., Janardhan Reddy, Y.C., Reess, T.J., Sakai, Y., Sato, J.R., Simpson, H.B., Soreni, N., Soriano-Mas, C., Spalletta, G., Stevens, M.C., Szeszko, P.R., Tolin, D.F., van Wingen, G.A., Venkatasubramanian, G., Walitza, S., Wang, Z., Yun, J.-.Y., Thompson, P.M., Stein, D.J., van den Heuvel, O.A.ENIGMA-OCD Working group, 2018. Cortical abnormalities associated with pediatric and adult obsessive-compulsive disorder: findings from the ENIGMA obsessive-compulsive disorder working group. Am. J. Psychiatry 175, 453–462. doi:10.1176/appi.ajp.2017.17050485.

Boileau, B., 2011. A review of obsessive-compulsive disorder in children and adolescents. Dialogues Clin. Neurosci. 13, 401–411.

Bolanos, C.A., Glatt, S.J., Jackson, D., 1998. Subsensitivity to dopaminergic drugs in periadolescent rats: a behavioral and neurochemical analysis. Dev. Brain Res. 111, 25–33. doi:10.1016/S0165-3806(98)00116-3.

Butwicka, A., Gmitrowicz, A., 2010. Symptom clusters in obsessive-compulsive disorder (OCD): influence of age and age of onset. Eur. Child Adolesc. Psychiatry 19, 365–370. doi:10.1007/s00787-009-0055-2.

Calabrese, E., Badea, A., Watson, C., Johnson, G.A., 2013. A quantitative magnetic resonance histology atlas of postnatal rat brain development with regional estimates of growth and variability. Neuroimage 71, 196–206. doi:10.1016/j.neuroimage.2013.01.017.

Calabrese, E., Johnson, G.A., 2013. Diffusion tensor magnetic resonance histology reveals microstructural changes in the developing rat brain. Neuroimage 79, 329–339. doi:10.1016/j.neuroimage.2013.04.101.

Calzà, J., Gürsel, D.A., Schmitz-Koep, B., Bremer, B., Reinholz, L., Berberich, G., Koch, K., 2019. Altered cortico – striatal functional connectivity during resting state in obsessive – compulsive disorder. Front. Psychiatry 10, 319. doi:10.3389/fpsyt.2019.00319.

Chen, Z., Zhang, H., Yushkevich, P.A., Liu, M., Beaulieu, C., 2016. Maturation along white matter tracts in human brain using a diffusion tensor surface model tract-specific analysis. Front. Neuroanat. 10, 9. doi:10.3389/fnana.2016.00009.

Christian, C.J., Lencz, T., Robinson, D.G., Burdick, K.E., Ashtari, M., Malhotra, A.K., Betensky, J.D., Szeszko, P.R., 2008. Gray matter structural alterations in obsessive-compulsive disorder: relationship to neuropsychological functions. Psychiatry Res 164, 123–131. doi:10.1016/j.pscychresns.2008.03.005.

Cox, R.W., 1996. AFNI : software for analysis and visualization of functional magnetic resonance neuroimages. Comput. Biomedial Res. 29, 162–173.

Del Casale, A., Kotzalidis, G.D., Rapinesi, C., Serata, D., Ambrosi, E., Simonetti, A., Pompili, M., Ferracuti, S., Tatarelli, R., Girardi, P., 2011. Functional neuroimaging in obsessive-compulsive disorder. Neuropsychobiology 64, 61–85. doi:10.1159/000325223.

Eilam, D., 2017. From an animal model to human patients: an example of a translational study on obsessive compulsive disorder (OCD). Neurosci. Biobehav. Rev. 76, 67–76. doi:10.1016/j.neubiorev.2016.12.034.

Eilam, D., Golani, I., Szechtman, H., 1989. D2-agonist quinpirole induces perseveration of routes and hyperactivity but no perseveration of movements. Brain Res 490, 255–267. doi:10.1016/0006-8993(89)90243-6.

Eisen, J.L., Sibrava, N.J., Boisseau, C.L., Mancebo, M.C., Stout, R.L., Pinto, A., Rasmussen, S.A., 2013. Five-year course of obsessive-compulsive disorder: predictors of remission and relapse. J. Clin. Psychiatry 74, 233–239. doi:10.4088/JCP.12m07657.

Fitzgerald, K.D., Welsh, R.C., Stern, E.R., Angstadt, M., Hanna, G.L., Abelson, J.L., Taylor, S.F., 2011. Developmental alterations of frontal-striatal-thalamic connectivity in obsessive compulsive disorder. J. Am. Acad. Child Adolesc. Psychiatry 50, 938–948. doi:10.1016/j.jaac.2011.06.011.

Frydman, I., de Salles Andrade, J.B., Vigne, P., Fontenelle, L.F., 2016. Can neuroimaging provide reliable biomarkers for obsessive-compulsive disorder? a narrative review. Curr. Psychiatry Rep 18, 90. doi:10.1007/s11920-016-0729-7.

Giannelli, M., Cosottini, M., Michelassi, M.C., Lazzarotti, G., Belmonte, G., Bartolozzi, C., Lazzeri, M., 2010. Dependence of brain DTI maps of fractional anisotropy and mean diffusivity on the number of diffusion weighting directions. J. Appl. Clin. Med. Phys. 11, 176–190.

Gilbert, A.R., Akkal, D., Almeida, J.R.C., Mataix-Cols, D., Kalas, C., Devlin, B., Birmaher, B., Phillips, M.L., 2009. Neural correlates of symptom dimensions in pediatric obsessive-compulsive disorder: a functional magnetic resonance imaging study. J. Am. Acad. Child Adolesc. Psychiatry 48, 936–944. doi:10.1097/CHI.0b013e3181b2163c.

Gruner, P., Vo, A., Ikuta, T., Mahon, K., Peters, B.D., Malhotra, A.K., Uluğ, A.M., Szeszko, P.R., 2012. White matter abnormalities in pediatric obsessive-compulsive disorder. Neuropsychopharmacology 37, 2730–2739. doi:10.1038/npp.2012.138.

Jenkinson, M., Bannister, P., Brady, M., Smith, S., 2002. Improved optimization for the robust and accurate linear registration and motion correction of brain images. Neuroimage 17, 825–841. doi:10.1006/nimg.2002.1132.

Jenkinson, M., Beckmann, C.F., Behrens, T.E.J., Woolrich, M.W., Smith, S.M., 2012. Fsl. Neuroimage 62, 782–790. doi:10.1016/j.neuroimage.2011.09.015.

Jenkinson, M., Smith, S., 2001. A global optimisation method for robust affine registration of brain images. Med. Image Anal. 5, 143–156. doi:10.1016/S1361-8415(01)00036-6.

Johansen-Berg, H., Behrens, T.E.J., 2013. Diffusion MRI: From Quantitative Measurement to In-Vivo Neuroanatomy, second ed. Elsevier/Academic Press.

Kessler, R.C., Berglund, P., Demler, O., Jin, R., Merikangas, K.R., Walters, E.E., 2005. Lifetime prevalence and age-of-onset distributions of DSM-IV disorders in the national domorbidity survey replication. Arch. Gen. Psychiatry 62, 593–602.

Koay, C.G., Chang, L., Carew, J.D., Pierpaoli, C., Basser, P.J., 2006. A unifying theoretical and algorithmic framework for least squares methods of estimation in diffusion tensor imaging. J. Magn. Reson. 182, 115–125. doi:10.1016/j.jmr.2006.06.020.

Koch, K., Reeß, T.J., Rus, O.G., Zimmer, C., Zaudig, M., 2014. Diffusion tensor imaging (DTI) studies in patients with obsessive-compulsive disorder (OCD): a review. J. Psychiatr. Res. 54, 26–35. doi:10.1016/j.jpsychires.2014.03.006.

Lázaro, L., Bargalló, N., Castro-Fornieles, J., Falcón, C., Andrés, S., Calvo, R., Junqué, C., 2009. Brain changes in children and adolescents with obsessive-compulsive disorder before and after treatment: a voxel-based morphometric MRI study. Psychiatry Res. - Neuroimaging 172, 140–146. doi:10.1016/j.pscychresns.2008.12.007.

Leckman, J.F., Denys, D., Simpson, H.B., Mataix-Cols, D., Hollander, E., Saxena, S., Miguel, E.C., Rauch, S.L., Goodman, W.K., Phillips, K.A., Stein, D.J., 2010. Obsessive-compulsive disorder: a review of the diagnostic criteria and possible subtypes for DSM-V. Depress. Anxiety 27, 507–527. doi:10.1002/da.20669.

Lochner, C., Stein, D.J., 2013. Heterogeneity of obsessive-compulsive disorder: a literature review. Harv. Rev. Psychiatry 11, 113–132. doi:10.1080/10673220303949.

Mangin, J.F., Poupon, C., Clark, C., Le Bihan, D., Bloch, I., 2002. Distortion correction and robust tensor estimation for MR diffusion imaging. Med. Image Anal. 6, 191–198. doi:10.1007/3-540-45468-3_23.

McCormick, P.N., Ginovart, N., Wilson, A.A., 2011. Isoflurane anaesthesia differentially affects the amphetamine sensitivity of agonist and antagonist D2/D3 positron emission tomography radiotracers: implications for in vivo imaging of dopamine release. Mol. Imaging Biol. 13, 737–746. doi:10.1007/s11307-010-0380-3.

Mengler, L., Khmelinskii, A., Diedenhofen, M., Po, C., Staring, M., Lelieveldt, B.P.F., Hoehn, M., 2014. Brain maturation of the adolescent rat cortex and striatum: changes in volume and myelination. Neuroimage 84, 35–44. doi:10.1016/j.neuroimage.2013.08.034.

Otte, W.M., van Meer, M.P.A., van der Marel, K., Zwartbol, R., Viergever, M.A., Braun, K.P.J., Dijkhuizen, R.M., 2015. Experimental focal neocortical epilepsy is associated with reduced white matter volume growth: results from multiparametric MRI analysis. Brain Struct. Funct. 220, 27–36. doi:10.1007/s00429-013-0633-4.

Paasonen, J., Stenroos, P., Salo, R.A., Kiviniemi, V., Gröhn, O., 2018. Functional connectivity under six anesthesia protocols and the awake condition in rat brain. Neuroimage 172, 9–20. doi:10.1016/j.neuroimage.2018.01.014.

Paxinos, G., Watson, W., 2005. The Rat Brain in Stereotaxic Coordinates, fifth ed. Elsevier Academic Press, Amsterdam.

Piras, Federica, Piras, Fabrizio, Chiapponi, C., Girardi, P., Caltagirone, C., Spalletta, G., 2015. Widespread structural brain changes in OCD: a systematic review of voxel-based morphometry studies. Cortex 62, 89–108. doi:10.1016/j.cortex.2013.01.016.

Posner, J., Marsh, R., Maia, T.V., Peterson, B.S., Gruber, A., Simpson, H.B., 2014. Reduced functional connectivity within the limbic cortico-striato-thalamo-cortical loop in unmedicated adults with obsessive-compulsive disorder. Hum. Brain Mapp. 35, 2852–2860. doi:10.1002/hbm.22371.

R Core Team, 2014. R: a language and environment for statistical computing.

Radua, J., Mataix-Cols, D., 2009. Voxel-wise meta-analysis of grey matter changes in obsessive-compulsive disorder. Br. J. Psychiatry 195, 393–402. doi:10.1192/bjp.bp.108.055046.

Sakai, Y., Narumoto, J., Nishida, S., Nakamae, T., Yamada, K., Nishimura, T., Fukui, K., 2011. Corticostriatal functional connectivity in non-medicated patients with obsessive-compulsive disorder. Eur. Psychiatry 26, 463–469. doi:10.1016/j.eurpsy.2010.09.005.

Servaes, S., Glorie, D., Stroobants, S., Staelens, S., 2019. Neuroreceptor kinetics in rats repeatedly exposed to quinpirole as a model for OCD. PLoS ONE 14, e0213313. doi:10.1371/journal.pone.0213313.

Servaes, S., Glorie, D., Verhaeghe, J., Stroobants, S., Staelens, S., 2017. Preclinical molecular imaging of glutamatergic and dopaminergic neuroreceptor kinetics in obsessive compulsive disorder. Prog. Neuro-Psychopharmacol. Biol. Psychiatry 77, 90–98. doi:10.1016/j.pnpbp.2017.02.027.

Smith, S.M., 2002. Fast robust automated brain extraction. Hum. Brain Mapp 17, 143–155. doi:10.1002/hbm.10062.

Song, C., Qu, Z., Blumm, N., Barabási, A.-.L., 2010. Limits of predictability in human mobility. Science 327 (80), 1018–1021. doi:10.1126/science.1177170.

Stuchlik, A., Radostová, D., Hatalova, H., Vales, K., Nekovarova, T., Koprivova, J., Svoboda, J., Horacek, J., 2016. Validity of quinpirole sensitization rat model of OCD: linking evidence from animal and clinical studies. Front. Behav. Neurosci. 10, 209. doi:10.3389/fnbeh.2016.00209.

Szechtman, H., Sulis, W., Eilam, D., 1998. Quinpirole induces compulsive checking behavior in rats: a potential animal model of obsessive-compulsive disorder (OCD). Behav. Neurosci. 112, 1475–1485. doi:10.1037/0735-7044.112.6.1475.

Taylor, S., 2011. Early versus late onset obsessive-compulsive disorder: evidence for distinct subtypes. Clin. Psychol. Rev. 31, 1083–1100. doi:10.1016/j.cpr.2011.06.007.

Teicher, M.H., Andersen, S.L., Hostetter, J.C., 1995. Evidence for dopamine receptor pruning between adolescence and adulthood in striatum but not nucleus accumbens. Dev. Brain Res. 89, 167–172. doi:10.1016/0165-3806(95)00109-Q.

Tucci, M.C., Dvorkin-Gheva, A., Sharma, R., Taji, L., Cheon, P., Peel, J., Kirk, A., Szechtman, H., 2014. Separate mechanisms for development and performance of compulsive checking in the quinpirole sensitization rat model of obsessive-compulsive disorder (OCD). Psychopharmacology (Berl) doi:10.1007/s00213-014-3505-6.

Ulloa, R.-.E., Nicolini, H., Fernández-Guasti, A., 2004. Age differences in an animal model of obsessive-compulsive disorder: participation of dopamine - Dopamine in an animal model of OCD. Pharmacol. Biochem. Behav. 78, 661–666. doi:10.1016/j.pbb.2004.04.009.

van Meer, M.P.A., Otte, W.M., van der Marel, K., Nijboer, C.H., Kavelaars, A., Berkelbach van der Sprenkel, J.W., Viergever, M.A., Dijkhuizen, R.M., 2012. Extent of bilateral neuronal network reorganization and functional recovery in relation to stroke severity. J. Neurosci. 32, 4495–4507. doi:10.1523/JNEUROSCI.3662-11.2012.

Veale, D., Roberts, A., 2014. Obsessive-compulsive disorder. BMJ 348, g2183. doi:10.1136/bmj.g2183.

Whitaker, N.G.G., Lindstrom, T.D., 1987. Disposition and biotransformation of quinpirole, a new D-2 dopamine agonist antihypertensive agent, in mice, rats, dogs and monkeys. Drug Metab. Dispos. 15, 107–113.

Zarei, M., Mataix-Cols, D., Heyman, I., Hough, M., Doherty, J., Burge, L., Winmill, L., Nijhawan, S., Matthews, P.M., James, A., 2011. Changes in gray matter volume and white matter microstructure in adolescents with obsessive-compulsive disorder. Biol. Psychiatry 70, 1083–1090. doi:10.1016/j.biopsych.2011.06.032.